Applied Physics Letters ARTICLE scitation.org/journal/apl

Generation of pure-state single photons with high heralding efficiency by using a three-stage nonlinear interferometer

Cite as: Appl. Phys. Lett. **116**, 204002 (2020); doi: 10.1063/5.0003601
Submitted: 3 February 2020 · Accepted: 8 May 2020 ·
Published Online: 21 May 2020

View Online Export Citation CrossMark

Jiamin Li,[1] Jie Su,[1] Liang Cui,[1,a)] Tianqi Xie,[1] Z. Y. Ou,[1,2] and Xiaoying Li[1,a)]

AFFILIATIONS

[1]College of Precision Instrument and Opto-Electronics Engineering, Key Laboratory of Opto-Electronics Information Technology, Ministry of Education, Tianjin University, Tianjin 300072, People's Republic of China
[2]Department of Physics, Indiana University-Purdue University Indianapolis, Indianapolis, Indiana 46202, USA

[a)]**Authors to whom correspondence should be addressed**: xiaoyingli@tju.edu.cn and lcui@tju.edu.cn

ABSTRACT

We experimentally study a fiber-based three-stage nonlinear interferometer and demonstrate its application in generating heralded single photons with high efficiency and purity by spectral engineering. We obtain a heralding efficiency of 90% at a brightness of 0.039 photons/pulse. The purity of the source is checked by two-photon Hong-Ou-Mandel interference with a visibility of 95 ± 6% (after correcting Raman scattering and multi-pair events). Our investigation indicates that the heralded source of single photons produced by the three-stage nonlinear interferometer has the advantages of high purity, high heralding efficiency, high brightness, and flexibility in wavelength and bandwidth selection.

Single photons are a fundamental resource for quantum optics and quantum information processing (QIP).[1] A single-photon state can be obtained by heralding on the detection of one of the photon pairs generated from spontaneous parametric processes.[2] Even with the advancement in producing good quality "on-demand" single-photon sources,[3,4] heralded single-photon sources are proven to be effective, economical, and most importantly of high quality.

The indistinguishability or modal purity is the most desired feature of a single-photon source and can be measured by Hong-Ou-Mandel (HOM) interference between two independent sources.[5] This interference phenomenon plays a key role in QIP, such as quantum teleportation[6,7] and linear optical quantum computing.[8] When the multi-pair events of signal and idler photon pairs are negligible, the visibility V of HOM interference between independent sources V and the indistinguishability of a heralded single-photon source characterized by the mode number M is related via $V = \frac{1}{M}$. For single photons in a well defined single-mode, i.e., $M = 1$, the ideal visibility with $V = 1$ is achievable. Another important criterion for characterizing the performance of single photons is the photon statistics measured by the second-order correlation function $g^{(2)}$. An ideal single-photon source corresponds to $g^{(2)} = 0$. For the source of heralded single photons, we have $g^{(2)} = \frac{2R_c}{h_s h_i}\left(1 + \frac{1}{M}\right)$,[9] where R_c denotes the production rate of single photons (in the unit of photons per pulse), $h_{s(i)}$ is referred to the heralding efficiency, which describes the probability of a single photon emerging at the signal (idler) band upon the detection event in the idler (signal) band. Therefore, to develop the high quality source of heralded single photons, both modal purity $M \to 1$ and high heralding efficiencies resulting in $h_s h_i \to 1$ are desirable.

For the pulse-pumped spontaneous parametric process, the precise timing provided by the ultra-short pump pulses brings convenience for synchronizing independent sources. However, the broadband nature of the pump field and strict phase matching condition in a highly dispersive nonlinear medium lead to complicated spectral correlation in the frequency domain. The existence of frequency correlation will degrade the purity of single photons.[5] To avoid this degradation, tremendous efforts were spent through the years. A straightforward approach is to apply passive narrow band filters to enforce single mode operation,[5] but at the cost of the reduction in brightness and product of heralding efficiencies $h_s h_i \ll 1$. Another approach is to specially engineer the nonlinear media with just the required dispersion to achieve single-mode operation without using a filter.[10–12] In this case, $M \approx 1$ and $h_s h_i \to 1$ are simultaneously attainable.[13–15] However, because nonlinear interaction and linear dispersion in nonlinear media are often mixed in parametric processes,

limited successes have been achieved so far only at some specific wavelengths with a sophisticated design.[16,17]

Recently, our group adopted an approach of engineering the quantum states with a nonlinear interferometer (NLI), whose fringe of quantum interference can be viewed as an active filter of photon pairs.[9,18] In a proof-of-principle experiment, using a two-stage NLI formed by two identical nonlinear fibers with a linear medium of single mode fiber (SMF) in between, we demonstrated that the spectra of photon pairs was engineered to nearly factorable states without sacrificing the product of $h_s h_i \to 1$. Exploiting the quantum interference of two pulse-pumped spontaneous four wave mixing (FWM) processes in nonlinear fibers, the spectra of photon pairs can be flexibly reshaped by dispersion engineering in the linear medium of SMF without affecting the phase matching condition of FWM.[9]

Furthermore, we showed theoretically that even better properties of the photon source can be achieved by implementing a multi-stage NLI (stage number $N > 2$) by a finer control of the phase shift of quantum interference.[9,18] Although such an idea was first proposed and analyzed by U'Ren *et al.*,[19] the proposed nano-structure of the nonlinear crystal is not easy to implement experimentally. In this paper, we experimentally realize a three-stage NLI with optical fibers, which make it relatively easy to extend to a higher stage number, and perform a two-photon HOM interference with two independent photon sources so produced to verify the high quality of the source.

Figure 1(a) shows the conceptual sketch of our three-stage NLI, consisting of three identical dispersion shifted fibers (DSFs) with two identical standard SMFs placed in between the DSFs. The DSFs with length L serve as the nonlinear media of spontaneous FWM, while the SMFs with length L_{DM} serve as the linear dispersive media with which we can engineer the spectrum of the generated photons. When the pump launched into the NLI is a Gaussian-shaped pulse train with a central frequency and bandwidth of ω_{p0} and σ_p, respectively, the joint spectral function (JSF) of the signal and idler photon pairs (ω_s, ω_i) emerging at the output of the NLI is expressed as[9]

$$F_{NLI}(\omega_s, \omega_i) = \exp\left[-(\omega_s + \omega_i - 2\omega_{p0})^2/4\sigma_p^2\right]\mathrm{sinc}(\Delta kL/2)H(\theta), \quad (1)$$

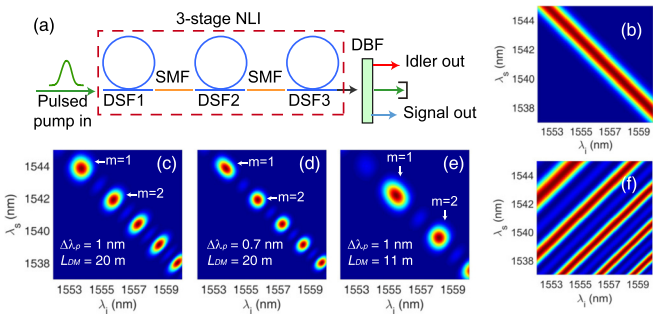

FIG. 1. (a) Conceptual sketch of a three-stage nonlinear interferometer (NLI) formed by dispersion-shifted fibers (DSFs) and standard single-mode fibers (SMFs). (b) The joint spectral intensity (JSI) of photon pairs directly out of DSF1 without interference. (c), (d), and (e) are the JSIs of photon pairs when the pump bandwidth and SMF length of the NLI are $\Delta\lambda_p = 1$ nm and $L_{DM} = 20$ m; $\Delta\lambda_p = 0.7$ nm and $L_{DM} = 20$ m; and $\Delta\lambda_p = 1$ nm and $L_{DM} = 11$ m, respectively. (f) Contour of the interference term $|H(\theta)|^2$ with the same parameters as those in (d).

with $\Delta k = \frac{k^{(2)}}{4}(\omega_s - \omega_i)^2 - 2\gamma P_p$ denoting the phase matching function in each DSF, where $H(\theta) = e^{j(N-1)\theta}\sin N\theta/\sin\theta$ results from interference for the N-stage NLI ($N = 3$ for our case), $k^{(2)} = \frac{\lambda_{p0}^2}{2\pi c}D_{slope}(\lambda_{p0} - \lambda_0)$ is the second order dispersion coefficient of the DSF, λ_{p0} is the central wavelength of the pump, c is the speed of light in vacuum, and D_{slope} is the dispersion slope of the DSF at zero dispersion wavelength (ZDW) λ_0. γ is the nonlinear coefficient of DSF, P_p is the peak power of the pump, $\theta = \frac{1}{2}(\Delta kL + \Delta\phi_{DM})$ with $\Delta\phi_{DM}$ being the part contributed by each linear medium, is the overall phase difference between the pump and photon pairs of adjacent DSFs.

The key in our design is that the phase difference $\Delta\phi_{DM}$ induced by the linear medium SMF is much greater than the phase mismatching term in the DSF or $\Delta kL/2 \ll 1$, so that the approximation

$$\theta \approx \Delta\phi_{DM}/2 = \lambda_{p0}^2 D_{SMF} L_{DM}(\omega_s - \omega_i)^2/16\pi c, \quad (2)$$

holds, where $D_{SMF} = 17\ \mathrm{ps/(nm \cdot km)}$ is the dispersion parameter of the SMF at the pump central wavelength λ_{p0}. In this case, the interference term $H(\theta)$ is dominated by the linear media.

To see the effect of interference, we simulate the spectral property of photon pairs by substituting the key parameters of our NLI into Eqs. (1) and (2). In the calculation, we set the parameters of the DSF as: $L = 150$ m, $\lambda_0 = 1548.5$ nm, $D_{slope} = 0.075\ \mathrm{ps/(km \cdot nm^2)}$, and $\gamma = 2\ \mathrm{W \cdot km^{-1}}$. The central wavelength and peak power of the pump are $\lambda_{p0} = 1548.8$ nm and $P_p = 0.35$ W. The joint spectral intensity (JSI) of photon pairs in Figs. 1(c)–1(e) is obtained when the 3 dB bandwidth of pump and SMF length of the NLI are (c) $\Delta\lambda_p = 1$ nm and $L_{DM} = 20$ m; (d) $\Delta\lambda_p = 0.7$ nm and $L_{DM} = 20$ m; and (e) $\Delta\lambda_p = 1$ nm and $L_{DM} = 11$ m, respectively. Compared to Fig. 1(b) without interference, the JSI is broken into islands with various shapes depending on the pump bandwidth $\Delta\lambda_p$ and the length of the linear dispersive medium L_{DM}. The the main maxima occur at $\theta = m\pi$ with $m = 1, 2, \ldots$ as the order number. Since the symmetry lines for the contours of the interference term $|H(\theta)|^2$ [Fig. 1(f)] and that of the pump envelope are orthogonal to each other [see Eqs. (1) and (2)], the shape of the island from which frequency uncorrelated photon pairs can be obtained should be round when the approximation $\mathrm{sinc}\left(\frac{\Delta kL}{2}\right) \approx 1$ holds.[9] When the condition $2\sigma_p^2 = \sigma_{int}^2 = 3c/2m\lambda_{p0}^2 D_{SMF} L_{DM}$ is satisfied, the m-th island becomes round shaped, where σ_{int} denotes the strip width of $|H(\theta)|^2$. We can then select the roundest one [$m = 1$ in (c) and $m = 2$ in (d) and (e)] for a factorized JSF with filters of the proper center wavelengths and bandwidths. Moreover, for the case of $\sigma_p < \frac{\sqrt{2}}{2}\sigma_{int}$, the m-th island corresponds to the frequency anti-correlated photon pairs [see m = 1 in (d) and (e)]; while for $\sigma_p > \frac{\sqrt{2}}{2}\sigma_{int}$, the m-th island corresponds to the frequency positive-correlated photon-pairs [see m ≥ 2 in (c)]. The results indicate that by changing the pump bandwidth and the length of the SMF, the wavelength and bandwidth of the pure state single photon with $h_s h_i \to 1$ can be flexibly adjusted within the gain bandwidth of FWM in the DSF.[20,21]

Good separation between the islands is desirable in order to select out the desired island by using filters.[9,18] However, the relative separation of the round shaped island in Figs. 1(c)–1(e) does not change with $\Delta\lambda_p$ and L_{DM} but will increase with the stage number N, as shown in Refs. 9 and 18. Here, we see well-separated islands even with $N = 3$, which is already better than the case of $N = 2$.[18] Note that U'Ren

et al.[19] had previously proposed the idea of generating a pure state single photon by using a sequential array of $\chi^{(2)}$-crystals gapped in between by linear dispersive media. However, since the amount of dispersion induced by each linear spacer and $\chi^{(2)}$ crystal is comparable, the approximation in Eq. (2) is not valid so that it requires a large number of $\chi^{(2)}$-crystals [large N in Eq. (1)] to separate different islands in the JSF similar to Figs. 1(c)–1(e). Because of the sophisticated structure, the proposal in Ref. 19 has not been experimentally realized yet.

The schematic of the experimental setup is shown in Fig. 2(a) where the gray shaded frames are heralded single photon sources (HSPS1 and HSPS2). The details of each HSPS is given in Fig. 1(a). The parameters of each HSPS are the same as those plotted in Fig. 1(c). The transmission loss of NLI is mostly due to imperfect fiber splicing: 3% loss at each splicing point. The NLI is submerged in liquid nitrogen to suppress Raman scattering.[22] The pump P_1 or P_2 is obtained by passing the output of a femoto-second fiber laser through a bandpass filter (F1) and 50/50 beam splitter (BS1). The repetition rate of the laser is about 36.8 MHz. The pulse duration of the pump with bandwidth of 1 nm is about 4 ps. Quarter ($\lambda/4$) and half wave plates ($\lambda/2$) placed in front of the polarization beam splitter (PBS1) are used to select the signal and idler photon pairs co-polarized with the pump and to reject the Raman-scattering (RS) cross-polarized with the pump.[22]

Because the nonlinearity of the fiber is weak, only about 0.04 photon pair is produced within a typical 4 ps duration pump pulse containing 10^7 photons. Thus, to reliably detect the correlated photon pairs, a high pump-to-signal rejection ratio is required. For HSPS1, we achieve this by passing the output of NLI through a dual-band filter (DBF1), which can separate the photon pairs from the pump with an isolation greater than 110 dB. The DBF is realized by cascading a tunable filter and a programmable optical filter (POF, model: Finisar Waveshaper 4000S), and the spectrum of DBF in each band is rectangularly shaped. The bandwidth of passband in both signal and idler fields can be adjusted from 0.1 nm to 1.5 nm, and the central wavelength of each band can be tuned from 1530 to 1570 nm. The signal and idler photons passing through DBF1 are detected by single photon detectors, SPD1 and SPD2. The SPDs are based on InGaAs avalanche diodes and operated at gated Geiger mode. The 2.5-ns-wide gate pulses arrive at the same rate of pump pluses, and the dead time of the gate is set to be 10 μs to suppress the after-pulse effect. The detection efficiency of each SPD is ~15%. The detection event of a photon in the signal (idler) band heralds the presence of a single photon in the idler (signal) band with the probability of $h_{i(s)}$.

We first verify the spectral property of photon pairs generated by the three-stage NLI. In the experiment, the pump power of P_1 is 50 μW and the bandwidth of DBF1 in both signal and idler bands is 0.1 nm. The two outputs of DBF1 (idler1 and signal1 fields) are directly coupled into SPD1 and SPD2, respectively. We measure both the twofold coincidence counts of the signal and idler photons originated from the same pump pulse and adjacent pulses, C^c and C^{acc}, when the central wavelengths of DBF1 in the signal (idler) channel are scanned from 1552.5 (1545) to 1558 (1539.5) nm with a step of 0.1 nm. Then, we deduce the true coincidence counts of photon pairs C^T by subtracting the measured C^{acc} from C^c. Figure 2(b) plots the contour map of C^T in the wavelength coordinates of λ_s and λ_i, which reflects the JSI of photon pairs. One sees that the contour map exhibits an "islands" pattern and agrees well with the theoretical prediction in Fig. 1(c).

We then measure the achievable heralding efficiency of the HSPS1. Note that in Fig. 2(b), the shape of island centering at 1543.8 and 1553.7 nm is round, indicating the spectral factorable property. By properly adjusting the DBF1, we select out this round shaped island to efficiently obtain uncorrelated photon pairs. Note that DBF1 is employed to select out the round shaped island, and it does not alter the spectra of the selected island when the filter bandwidth is optimized. The spectra-reshaping is done by the two-photon interference effect in NLI. In this experiment, the bandwidth of each band is adjusted to be 1.5 nm [see the dashed lines in Fig. 2(b)], and the overall detection efficiencies (including the efficiencies of SPDs and DBF1) in the signal and idler bands are $\eta_s = 4.1\%$ and $\eta_i = 4.3\%$, respectively. During the measurement, we record the single counts of the individual signal and idler fields and the twofold coincidence counts of two fields under different pump powers. For each pump power level, we subtract C^{acc} to obtain the true coincidence counting rate $C^T = C^c - C^{acc}$. The measured data of single counts in the signal (idler) band is fitted with $N_{s(i)} = s_1 P_{ave} + s_2 P_{ave}^2$, where P_{ave} is the average pump power, and s_1 and s_2 are the fitting parameters. $s_1 P_{ave}$ and $s_2 P_{ave}^2$, respectively, correspond to the intensities of spontaneous Raman scattering and FWM in the NLI.[22] The results are shown in Fig. 3(a) where the dashed and dotted lines are $s_1 P_{ave}$ and $s_2 P_{ave}^2$, respectively. We then deduce the collection efficiency $\xi'_{s(i)}$, which describes the probability of detecting the photon at the signal (idler) band for a photon detected in the idler (signal) band. In general, there is a relation between the collection efficiency and heralding efficiency: $h_{s(i)} = \xi'_{s(i)}/\eta_{s(i)}$.[9] To directly show that the purity and efficiency of HSPS will benefit from the improvement of photon pairs' collection efficiencies, here we correct the measured collection efficiency with the detection efficiency, i.e.,

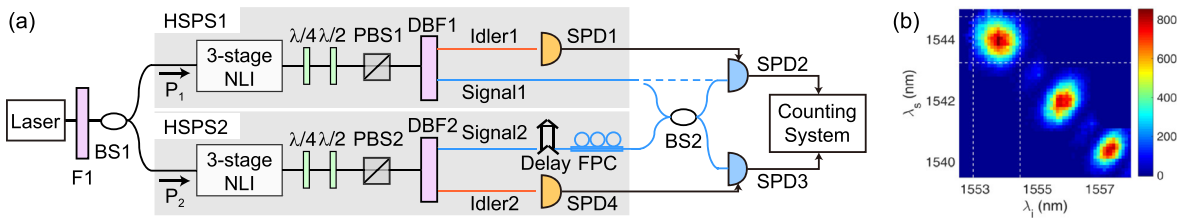

FIG. 2. (a) Experimental setup of two-photon HOM interference by using two heralded single photon sources (HSPS1 and HSPS2). The shaded areas are HSPS1 and HSPS2, whose details are given in Fig. 1(a). P1-P2, pulsed pump; NLI, nonlinear interferometer; F, filter; DBF, dual-band filter; FPC, fiber polarization controller; BS, 50/50 beam splitter; and SPD, single photon detector. (b) Contour map of true coincidence of photon pairs as a function of λ_s and λ_i, reflecting the joint spectral intensity of photon pairs.

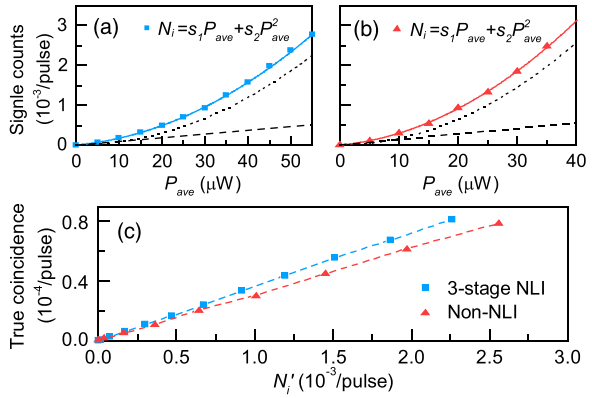

FIG. 3. (a) and (b) are the counting rates of SPD1 for individual idler band vs the average pump power P_{ave} for the three-stage NLI and non-NLI (single piece 450-m long DSF) cases, respectively. The second-order polynomials $N_i = s_1 P_{ave} + s_2 P_{ave}^2$ (solid curves) are used to fit the data in plots (a) and (b). The linear and quadratic terms of the fitting functions are represented by the dashed and dotted lines, respectively. (c) The true coincidence rate vs the counting rate $N_i' = s_2 P_{ave}^2$ of idler photons originated from the FWM in two cases.

$\xi_{s(i)} = \frac{\xi'_{s(i)}}{\eta_{s(i)}} = \frac{C^T}{\eta_{i(s)} N'_{i(s)}} = h_{s(i)}$, where $N'_{s(i)} = s_2 P_{ave}^2$ is the quadratic part of $N_{s(i)}$.[9,23] Indeed, such a correction is reasonable because the total detection efficiencies of our experimental system can in principle be improved up to 95% by upgrading the SPDs and DBFs.[24,25] The measured results indicate that the achievable heralding efficiencies h_s and h_i are about 91.2% and 90.5%. As a comparison, we repeat the efficiency measurement [Fig. 3(b)] by replacing the NLI with a single piece 450-m long DSF (referred to as the non-NLI case), which is realized by removing the SMFs placed in the NLI and directly connecting three DSFs. From the results of measurement, we find that the collection efficiencies of ξ_s and ξ_i are about 67.1% and 70.1% for the non-NLI case. Figure 3(c) clearly illustrates that the collection efficiency of signal and idler photon pairs is improved by the NLI.

The detection event of SPD1 in the idler output band of the NLI is expected to herald the presence of single photons in the signal band. The photon statistical property of HSPS1, is characterized by $g^{(2)}$, the intensity correlation function of the heralded single photons. To measure $g^{(2)}$, the heralded photons in signal1 field are sent into a Hanbury Brown–Twiss (HBT) interferometry consisting of a beam splitter (BS2) and two detectors (SPD2 and SPD3). During the measurement, we record the single counts of SPD1 (N_i), threefold coincidence counts of SPD1, SPD2, and SPD3 (N_{123}), and twofold coincidence counts between SPD1 and SPD2 (SPD3) (N_{12} and N_{13}). The value $g^{(2)}$ is deduced from the relation: $g^{(2)} = \frac{N_{123} N_i}{N_{12} N_{13}}$. Figure 4(a) shows the measured $g^{(2)}$ as a function of pump power. One sees that $g^{(2)}$ increases with the pump power. This is due to multi-pair events whose probability increases as the pump power or production rate of photon pairs. At the pump power of 30 μW, corresponding to a photon pair production rate of about 0.015 pairs/pulse (after correcting Raman scattering), the $g^{(2)}$ of HSPS1 is about 0.034 ± 0.012, which is significantly less than the classical limit of 1. Even when the production rate is increased to 0.043 pairs/pulse (under the pump power of 50 μW), the value of $g^{(2)} = 0.219 \pm 0.008$ is still well below the classical limit of 1, which clearly illustrates the non-classical nature of our single photon source.

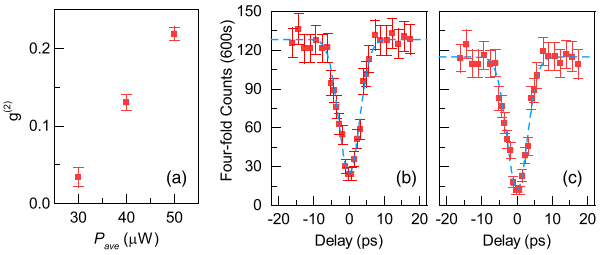

FIG. 4. (a) Intensity correlation function $g^{(2)}$ of HSPS vs the average pump power P_{ave}. (b) The raw data (with only dark counts of SPDs subtracted) and (c) corrected data (Raman noise subtracted) of fourfold coincidences as a function of the relative delay between the two HSPS. The dashed line is the fitting to a Gaussian function.

Finally, we verify the modal purity of HSPS1 by building another HSPS (HSPS2) and performing two-photon HOM interference measurement between the two independent HSPSs [see Fig. 2(a)]. The two HSPSs are identical. The detection event of SPD1 (SPD4) in the idler1 (idler2) field heralds the presence of a single photon in the signal1 (signal2) field. In this experiment, the outputs of the two HSPSs (signal1 and signal2) are carefully path matched and simultaneously fed into a 50/50 fiber beam splitter (BS2) from two input ports, respectively. Before sending to BS2, the output of HSPS2 (signal2 field) is delayed by a translation stage. To ensure the two input fields of BS2 have the identical polarization, the polarization of the signal2 field is properly adjusted by a fiber polarization controller (FPC). Note that SPD3 and SPD4 are the same as SPD1 and SPD2, except that their quantum efficiencies are slightly different. During the measurement, the pump powers of both P1 and P2 are about 50 μW, and the production rate of heralded single photons is about 0.039 photons/pulse. The overall detection efficiency for the signal and idler photons (including insertion loss of DBF1 or DBF2) is ~5%. We record the fourfold coincidences of four SPDs vs the position of the translation stage. The raw data (after subtracting the dark counts of SPDs) is plotted in Fig. 4(b), showing that the visibility of the HOM interference is 81% ± 6%.

For an ideal single photon state, there is no need to modify the measured fourfold coincidences if the dark counts of the SPDs have been subtracted. But for the heralded single photon state generated from the fiber, background counts caused by Raman scattering and the multi-pair events originated from FWM should be subtracted as well. We first correct the influence of Raman scattering, whose photon number can be extracted from the linear term ($s_1 P_{ave}$) in Fig. 3(a). Since the strength of the Raman scattering is quite weak, the impact of Raman scattering upon the visibility V is similar to that of the dark counts of SPDs. It is straightforward to obtain the visibility after correction of the Raman effect: $V \approx (90 \pm 6)\%$. We then analyze the degradation of V due to multi-pair events by using Eq. (12) in Ref. 26 according to the deduced brightness of HSPS (0.039 photons/pulse) in the measurement and find the result after correction is $V \approx (95 \pm 6)\%$.

In addition to the HOM interference measurement, we characterize the mode number of an individual signal field for NLI by measuring its intensity correlation function $g_s^{(2)}$. In this measurement, the pump of HSPS2 (P2) is blocked and only the twofold coincidence counts of SPD2 and SPD3 are analyzed by our counting system. The directly measured result is $g_s^{(2)} = 1.8$. But after correcting the contribution from Raman scattering,[18] we find that the intensity correlation

function for the signal field via FWM is $g_s^{(2)} = 1.96$,[18,27] which is consistent with the result $g_s^{(2)} = 1.97$, obtained from the singular value decomposition of JSI in Fig. 2(b) under the assumption of a flat spectral phase. The detailed correction method and procedure can be found in Refs. 18 and 27. Note that the corrected result of $g_s^{(2)}$ would be directly measurable if the NLI was cooled with liquid helium.[28] Our analysis illustrates that the mode number of $M = 1.04$ can be deduced with $M = 1/(g_s^{(2)} - 1)$.[29] Hence, the corrected visibility V and deduced mode number M are consistent with the relation $V = 1/M$.

In conclusion, we experimentally study an NLI containing three nonlinear media. Our investigation indicates that the performance of a pulse-pumped three-stage NLI is better than that of a two-stage NLI[18] in engineering the spectral property of photon pairs. We demonstrate that the three-stage NLI can be used to develop a pure state of heralded single photons with a high heralding efficiency. When the brightness and heralding efficiency of each telecom band HSPS are about 0.039 photons/pulse and 90%, respectively, the raw data for the visibility of two-photon HOM interference between two independent HSPSs is measured to be 81% ± 6%. After correcting the Raman scattering and multi-pair events, the visibility can reach 95% ± 6%. Our results show that the heralded single photons generated from the three-stage NLI simultaneously have the advantages of high purity, high heralding efficiency, high brightness, and flexibility in wavelength and bandwidth selection. Moreover, we note that the performance of our HSPSs is robust to the structure fluctuations of the NLI, because we do not observe any change in the key performance parameters of the HSPSs when the lengths of DSF and SMF in the NLI are varied within a few centimeters. We believe that the fiber-based multi-stage nonlinear interferometer, which is easy to implement, will be a useful resource for quantum information processing involving quantum interference among multiple independent sources. Furthermore, the method of engineering the spectra of photon states using the multi-stage NLI also applies to other experimental platforms, which are based on a parametric process in nonlinear media, as long as the internal loss of the NLI can be well controlled.

The work was supported in part by the National Natural Science Foundation of China (Nos. 11527808, 91736105, and 11874279) and the Science and Technology Program of Tianjin (No. 18ZXZNGX00210).

REFERENCES

[1]S. Slussarenko and G. J. Pryde, "Photonic quantum information processing: A concise review," Appl. Phys. Rev. **6**, 041303 (2019).
[2]C. Hong and L. Mandel, "Experimental realization of a localized one-photon state," Phys. Rev. Lett. **56**, 58–60 (1986).
[3]C. Santori, D. Fattal, J. Vuckovic, G. S. Solomon, and Y. Yamamoto, "Indistinguishable photons from a single-photon device," Nature **419**, 594–597 (2002).
[4]X. Ding, Y. He, Z.-C. Duan, N. Gregersen, M.-C. Chen, S. Unsleber, S. Maier, C. Schneider, M. Kamp, S. Höfling, C.-Y. Lu, and J.-W. Pan, "On-demand single photons with high extraction efficiency and near-unity indistinguishability from a resonantly driven quantum dot in a micropillar," Phys. Rev. Lett. **116**, 020401 (2016).
[5]Z. Y. Ou, J. K. Rhee, and L. J. Wang, "Photon bunching and multiphoton interference in parametric down-conversion," Phys. Rev. A **60**, 593–604 (1999).
[6]D. Bouwmeester, J. Pan, M. Klaus, E. Manfred, W. Harald, and Z. Anton, "Experimental quantum teleportation," Nature **390**, 575–579 (1997).
[7]L.-M. Duan, M. Lukin, J. I. Cirac, and P. Zoller, "Long-distance quantum communication with atomic ensembles and linear optics," Nature **414**, 413–418 (2001).
[8]E. Knill, R. Laflamme, and G. J. Milburn, "A scheme for efficient quantum computation with linear optics," Nature **409**, 46–52 (2001).
[9]J. Su, J. Li, L. Cui, X. Li, and Z. Y. Ou, "Quantum state engineering by nonlinear quantum interference," arXiv:1811.07646v2 (2018).
[10]F. Kaneda, K. Garay-Palmett, A. B. U'Ren, and P. G. Kwiat, "Heralded single-photon source utilizing highly nondegenerate, spectrally factorable spontaneous parametric downconversion," Opt. Express **24**, 10733–10747 (2016).
[11]F. Graffitti, P. Barrow, M. Proietti, D. Kundys, and A. Fedrizzi, "Independent high-purity photons created in domain-engineered crystals," Optica **5**, 514–517 (2018).
[12]R. J. Francis-Jones, R. A. Hoggarth, and P. J. Mosley, "All-fiber multiplexed source of high-purity single photons," Optica **3**, 1270–1273 (2016).
[13]W. P. Grice, A. B. U'ren, and I. A. Walmsley, "Eliminating frequency and space-time correlations in multiphoton states," Phys. Rev. A **64**, 063815 (2001).
[14]P. J. Mosley, J. S. Lundeen, B. J. Smith, P. Wasylczyk, A. B. U'Ren, C. Silberhorn, and I. A. Walmsley, "Heralded generation of ultrafast single photons in pure quantum states," Phys. Rev. Lett. **100**, 133601 (2008).
[15]L. Cui, X. Li, and N. Zhao, "Minimizing the frequency correlation of photon pairs in photonic crystal fibers," New J. Phys. **14**, 123001 (2012).
[16]P. G. Evans, R. S. Bennink, W. P. Grice, T. S. Humble, and J. Schaake, "Bright source of spectrally uncorrelated polarization-entangled photons with nearly single-mode emission," Phys. Rev. Lett. **105**, 253601 (2010).
[17]A. M. Brańczyk, A. Fedrizzi, T. M. Stace, T. C. Ralph, and A. G. White, "Engineered optical nonlinearity for quantum light sources," Opt. Express **19**, 55–65 (2011).
[18]J. Su, L. Cui, J. Li, Y. Liu, X. Li, and Z. Y. Ou, "Versatile and precise quantum state engineering by using nonlinear interferometers," Opt. Express **27**, 20479–20492 (2019).
[19]A. U'Ren, C. Silberhorn, K. Banaszek, I. Walmsley, R. Erdmann, W. Grice, and M. Raymer, "Generation of pure-state single-photon wavepackets by conditional preparation based on spontaneous parametiric downconversion," Laser Phys. **15**, 146–161 (2005).
[20]J. Hansryd and P. A. Andrekson, "Broad-band continuous-wave-pumped fiber optical parametric amplifier with 49-DB gain and wavelength-conversion efficiency," IEEE Photonics Technol. Lett. **13**, 194–196 (2001).
[21]X. Li, X. Ma, Z. Y. Ou, L. Yang, L. Cui, and D. Yu, "Spectral study of photon pairs generated in dispersion shifted fiber with a pulsed pump," Opt. Express **16**, 32–44 (2008).
[22]X. Li, J. Chen, P. Voss, J. Sharping, and P. Kumar, "All-fiber photon-pair source for quantum communications: Improved generation of correlated photons," Opt. Express **12**, 3737–3744 (2004).
[23]L. Yang, X. Ma, X. Guo, L. Cui, and X. Li, "Characterization of a fiber-based source of heralded single photons," Phys. Rev. A **83**, 053843 (2011).
[24]D. V. Reddy, A. E. Lita, S. W. Nam, R. P. Mirin, and V. B. Verma, "Achieving 98% system efficiency at 1550 nm in superconducting nanowire single photon detectors," in Rochester Conference on Coherence and Quantum Optics (CQO-11) 2019, p. W2B.2.
[25]Y. O. Usenko, A. R. Gizatulin, and A. K. Sultanov, "Improving the fiber Bragg grating apodization efficiency in the DWDM systems," Proc. SPIE **11146**, 1114604 (2019).
[26]X. Ma, L. Cui, and X. Li, "Hong-ou-mandel interference between independent sources of heralded ultrafast single photons: Influence of chirp," J. Opt. Soc. Am. B **32**, 946–954 (2015).
[27]J. Su, J. Li, L. Cui, X. Li, and Z. Y. Ou, "Interference between two independent multi-temporal-mode thermal fields," Phys. Rev. A **99**, 013838 (2019).
[28]S. D. Dyer, B. Baek, and S. W. Nam, "High-brightness, low-noise, all-fiber photon pair source," Opt. Express **17**, 10290–10297 (2009).
[29]N. Liu, Y. Liu, X. Guo, L. Yang, X. Li, and Z. Y. Ou, "Approaching single temporal mode operation in twin beams generated by pulse pumped high gain spontaneous four wave mixing," Opt. Express **24**, 1096–1108 (2016).